International Journal of Heat and Mass Transfer 235 (2024) 126155

Contents lists available at ScienceDirect

International Journal of Heat and Mass Transfer

journal homepage: www.elsevier.com/locate/hmt

Linearly unstable forced and free flow in an anisotropic porous channel

A. Barletta [a,*], M. Celli [a], P.V. Brandão [a], S. Lazzari [b], E. Ghedini [a]

[a] Department of Industrial Engineering, Alma Mater Studiorum Università di Bologna, Viale Risorgimento 2, 40136 Bologna, Italy
[b] Department of Architecture and Design, Università di Genova, Stradone S. Agostino 37, 16123 Genova, Italy

ARTICLE INFO

Keywords:
Mixed convection
Porous medium
Anisotropy
Uniform heating/cooling
Linear instability

ABSTRACT

The combined forced and free convection flow in a horizontal porous channel saturated by a fluid is studied. The boundary walls are considered as uniformly heated-cooled with symmetric heat fluxes. The horizontal porous layer is modelled as anisotropic with different permeabilities in the horizontal and vertical directions. A fully-developed stationary flow in the porous channel exists, endowed with a temperature gradient inclined to the vertical. This basic stationary flow turns out to become linearly unstable when the Rayleigh number is sufficiently high, with a neutral stability condition strongly dependent on the Péclet number associated with the basic flow rate. A minimum Péclet number exists below which no linear instability arises. A streamfunction formulation is introduced to test the behaviour of the small-amplitude perturbations. The stability eigenvalue problem is solved numerically for different Péclet numbers and anisotropy ratios in order to evaluate the neutral stability threshold and the critical values for the onset of the linear instability.

1. Introduction

The onset of thermal instability in fluid saturated porous layers has been the subject of a wide research effort over several years. Within such a topic, the pioneering papers by Horton and Rogers [1] and by Lapwood [2] identified the basic features of the instability. These authors studied and solved the now well-known Horton–Rogers–Lapwood (HRL), or Darcy–Bénard, problem. In particular, they determined the critical value of the Rayleigh number for the onset of thermal convection for a porous layer heated from below (*i.e.*, the porous medium counterpart of the classical Rayleigh–Bénard problem). For the HRL problem, the basic stationary solution whose stability is investigated is a rest state with a purely vertical temperature gradient, just like the Rayleigh–Bénard problem. In fact, the governing parameter defining the linear instability threshold is a modified Rayleigh number based on the permeability of the porous medium and called by many authors the Darcy–Rayleigh number. Prats [3] reconsidered the HRL problem by including a basic horizontal throughflow and found that the net mass flow rate does not have any influence on the critical value of the Darcy–Rayleigh number for the onset of thermal convection.

For a horizontal porous channel bounded by impermeable parallel plane walls, when symmetric wall heat fluxes (a uniform wall heating or cooling) are considered, a rest basic stationary state does not exist unless a nonzero mass flow rate must is prescribed. Indeed, a nonzero flow rate may ensure the closure of the energy balance under stationary conditions. When combined with a prescribed horizontal pressure gradient, the symmetric wall heat flux boundary conditions yield a temperature gradient with both a vertical and a horizontal component. The stability of this configuration has been investigated by Barletta [4]. Further stability analyses on similar basic states were carried out by Sphaier and Barletta [5], by Barletta et al. [6], by Sphaier et al. [7] and by Barletta and Rees [8]. These conditions of basic flow, where an inclined temperature gradient drives the instability, are included in the more general topic of Hadley-like flows [9]. The pivotal studies in this area had been carried out by Weber [10], Nield [11,12], Kaloni and Qiao [13] and by Qiao and Kaloni [14].

The analysis proposed by Barletta [4] is relative to an isotropic porous layer, *i.e.*, a solid phase with the same value of permeability in every direction. On the other hand, anisotropic porous materials are quite common in practical cases. For instance, the rapidly developing area of additive manufacturing techniques allows an undemanding production of anisotropic porous layers with specified properties. Incidentally, we mention that the fabrication of either isotropic or anisotropic porous layers having reproducible properties is a goal for the developing industry of compact heat exchangers, where the limitations in the use of metallic foams for the heat transfer enhancement are often linked to the hardly reproducible morphology of such foams. In fact, the role of anisotropy in porous media in the onset of thermal instability has been the subject of several recent studies [15–21].

The present work aims to investigate how the anisotropy in the porous structure may influence the onset of thermal instability for a

* Corresponding author.
E-mail address: antonio.barletta@unibo.it (A. Barletta).

https://doi.org/10.1016/j.ijheatmasstransfer.2024.126155
Received 17 May 2024; Received in revised form 24 August 2024; Accepted 31 August 2024
Available online 5 September 2024

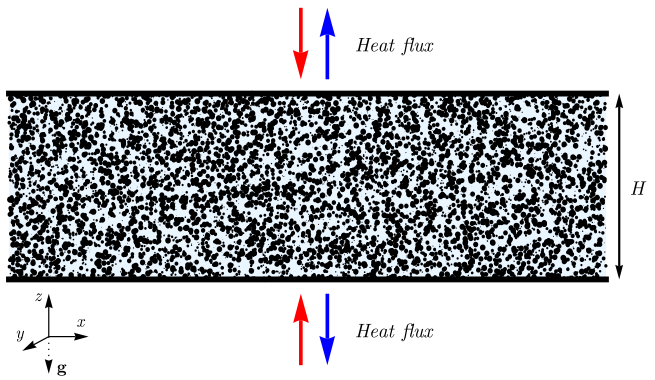

Fig. 1. A sketch of the saturated porous channel and of the thermal boundary conditions.

porous channel with symmetric wall heat fluxes, thus extending the analysis carried out by Barletta [4]. To achieve this goal, two different values of the permeability are considered: one for the vertical direction and one for both the horizontal directions. The linear stability of this system is investigated by solving the eigenvalue problem obtained by using the normal modes method. In order to rationalise the mathematical procedure, an arbitrarily inclined horizontal through flow with respect to a given reference frame is devised. This approach allows one to map the fully three-dimensional problem onto a two-dimensional problem involving a parameter, i.e., the inclination angle. Since the stability problem is two-dimensional, a streamfunction-temperature formulation can be employed. Both the neutral stability curves and the critical values of the Darcy–Rayleigh number are determined as functions of the inclination angle, of the Péclet number (measuring the strength of the horizontal flow rate) and of the dimensionless parameter describing the anisotropy.

The importance of the configuration examined in this paper, where either a net wall heating or cooling is supplied to the fluid, is due to its manifold applications. For instance, one may devise the cooling of electronic devices. For such systems, where printed circuit boards are modelled as an array of parallel heat-generating plates, cooling may be effectively carried out by forced or mixed convection flow in the channels separating two neighbouring plates. The heat transfer rate can be enhanced by utilising metal foams and, hence, by the convective flow in a fluid saturated porous medium. Besides this specific example, forced or mixed convection channel flows under conditions of net wall heating define a classical problem of heat transfer. We mention that the book by Shah and London [22] classifies wall heating boundary conditions under the variants H1 and H2.

2. Mathematical model

Let us consider a fluid saturated porous layer with height H and an infinite width in both horizontal x and y directions. Such a layer is heated/cooled from below and above by symmetric and uniform heat fluxes prescribed at the impermeable boundaries $z = 0, H$ (see Fig. 1). The red/blue arrows in Fig. 1 mean that both channel walls can either be heated (red) or cooled (blue). We also consider a net mass flow rate imposed along the x direction. In order to investigate the onset of thermal convection, we model the local momentum balance equation by employing Darcy's law where the buoyancy force is taken into account and the Oberbeck–Boussinesq approximation is employed [23]. Thus, we assume local balance equations for mass, momentum and energy given by

$$\boldsymbol{\nabla}\cdot\mathbf{u}=0,$$
$$\frac{\mu}{K_h}u=-\frac{\partial p}{\partial x},\quad \frac{\mu}{K_h}v=-\frac{\partial p}{\partial y},\quad \frac{\mu}{K_z}w=-\frac{\partial p}{\partial z}+\rho_0\,g\,\beta(T-T_0),$$
$$\rho_0\,c\left(\sigma\frac{\partial T}{\partial t}+\mathbf{u}\cdot\boldsymbol{\nabla}T\right)=\chi\nabla^2T,$$
$$z=0:\qquad w=0,\quad -\chi\frac{\partial T}{\partial z}=q_0,$$
$$z=H:\qquad w=0,\quad \chi\frac{\partial T}{\partial z}=q_0,\tag{1}$$

where $\mathbf{u}=(u,v,w)$ is the seepage velocity, p is the local difference between the pressure and the hydrostatic pressure, T is the temperature, t is the time, (x,y,z) are the Cartesian coordinates, μ is the dynamic viscosity of the fluid, K_h and K_z are, respectively, the permeabilities in the horizontal and the vertical directions, ρ_0 is the fluid density evaluated at the reference temperature T_0, g is the modulus of the gravitational acceleration $\mathbf{g}$, β is the thermal expansion coefficient of the fluid, c is the specific heat capacity of the fluid, σ is the ratio between the average volumetric heat capacity of the porous medium and the volumetric heat capacity of the fluid, χ is the effective thermal conductivity of the porous medium evaluated as the average value of the conductivities for the solid and fluid phases weighted by the porosity, and q_0 is the heat flux prescribed at the boundaries (either positive or negative).

It must be mentioned that, although the permeability of the porous material has been modelled as anisotropic and, hence, represented by a tensor, the thermal conductivity has been considered isotropic and, hence, represented by a scalar. The motivation for such a choice relies on the nature of the thermal conductivity χ as an effective thermal conductivity resulting from a local volume average of the solid and fluid conductivities. In fact, the effective thermal conductivity averages over the reference elementary volume and over the different directions within such a volume. Thus, the modelling of χ as a scalar quantity is justified conceptually giving also the advantage of a simplified model to ground our forthcoming results. We mention that a model similar to that expressed with (1) has been employed in the classical papers by Tyvand and Storesletten [24] and by Trew and McKibbin [25], as well as in the recent studies by Storesletten and Rees [15] and by Barletta and Celli [26].

A dimensionless formulation of the governing equation is obtained by defining the following scaling:

$$\frac{(x,y,z)}{H}\to(x,y,z),\quad \frac{\chi}{\rho_0\,c\,H^2\sigma}t\to t,\quad \frac{\rho_0\,c\,H}{\chi}\mathbf{u}\to\mathbf{u},\quad \frac{\rho_0\,c\,K_h}{\chi\,\mu}p\to p,$$
$$\frac{T-T_0}{\Delta T}\to T,\qquad \text{for}\quad \Delta T=\frac{\chi\mu}{\rho_0^2\,c\,\beta\,g\,K_h\,H}.\tag{2}$$

Thus, Eqs. (1) can be rewritten as

$$\boldsymbol{\nabla}\cdot\mathbf{u}=0,$$
$$u=-\frac{\partial p}{\partial x},\quad v=-\frac{\partial p}{\partial y},\quad w=-a\frac{\partial p}{\partial z}+aT,$$
$$\frac{\partial T}{\partial t}+\mathbf{u}\cdot\boldsymbol{\nabla}T=\nabla^2T,$$
$$z=0:\qquad w=0,\quad \frac{\partial T}{\partial z}=-Ra,$$
$$z=1:\qquad w=0,\quad \frac{\partial T}{\partial z}=Ra,\tag{3}$$

where Ra is the Darcy–Rayleigh number and a is the anisotropy ratio,

$$Ra=\frac{\rho_0^2\,c\,\beta\,g\,K_h\,H^2q_0}{\chi^2\mu},\quad a=\frac{K_z}{K_h}.\tag{4}$$

Hereafter, the Darcy–Rayleigh number will be called Rayleigh number for the sake of brevity. Since q_0 might be either positive (heating) or negative (cooling), the Rayleigh number can assume either a positive or a negative value.

2.1. Basic state

A stationary solution of (3), *i.e.* a basic state, exists given by

$$\mathbf{u}_b=\left(\cos\varphi\,\mathbf{e}_x+\sin\varphi\,\mathbf{e}_y\right)F(z),$$

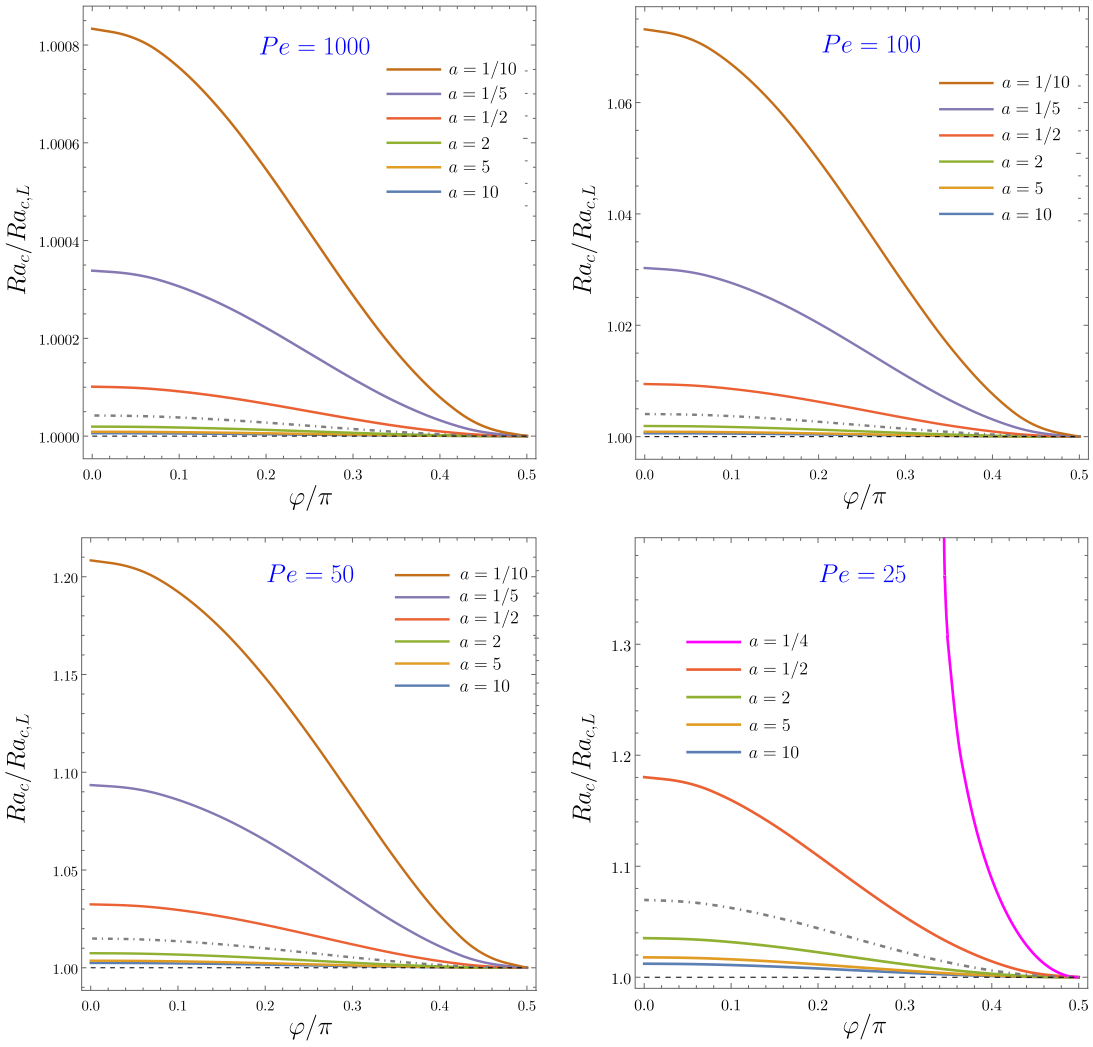

Fig. 2. Ratio between Ra_c for oblique modes and for longitudinal modes, $Ra_{c,L}$, versus φ/π for different Pe and anisotropy ratios a. The grey dashed–dotted lines identify the isotropic case, $a = 1$. The black thin dashed lines identify the value 1 for the Ra_c ratio.

$$\boldsymbol{\nabla} T_b = \frac{2Ra}{Pe}\left(\cos\varphi\,\mathbf{e}_x + \sin\varphi\,\mathbf{e}_y\right) + G(z)\,\mathbf{e}_z, \quad \boldsymbol{\nabla} p_b = \left(-u_b, -v_b, T_b\right),$$

$$\text{for} \quad F(z) = Pe - \frac{Ra(2z-1)}{Pe}, \quad G(z) = Ra(2z-1) - \frac{2Ra^2\left(z^2-z\right)}{Pe^2}, \tag{5}$$

where the subscript "b" stands for "basic state", while $\mathbf{e}_x, \mathbf{e}_y$ and $\mathbf{e}_z$ denote the unit vectors along the (x, y, z) axes. The Péclet number, Pe, is defined so that it yields the dimensionless mean velocity along the flow direction,

$$Pe = \int_0^1 \mathbf{u}_b \cdot \mathbf{n}\,\mathrm{d}z, \quad \text{for} \quad \mathbf{n} = \cos\varphi\,\mathbf{e}_x + \sin\varphi\,\mathbf{e}_y. \tag{6}$$

Eq. (5) describes a horizontal unidirectional flow along the $\mathbf{n}$ direction. This solution is singular when $Pe \to 0$. Such a singularity had to be expected as a stationary solution is impossible with a net heating/cooling from the boundaries, unless a net flow rate is prescribed along a horizontal direction. We mention that this basic state is exactly the same considered by Barletta [4] in the case of a perfectly isotropic porous medium. In fact, the basic solution (5) is independent of the anisotropy parameter a.

Considering a general mixed convection stationary solution with the flow direction inclined an angle φ to the x axis serves, in the linear instability analysis, to explore the action of an oblique wavelike perturbation directed along the x axis. Such oblique perturbation modes are general on varying φ in the interval $[0, \pi/2]$. In particular, $\varphi = 0$ defines transverse modes, while $\varphi = \pi/2$ yields longitudinal modes. We also mention that, strictly speaking, the temperature T_b in the basic state is defined only up to an arbitrary additive constant. This is a consequence of the governing model (3) being formulated only in terms of the temperature derivatives, except for the z component of the local momentum balance equation. On the other hand, this equation may just yield an extra linear term in the basic pressure field p_b which, however, does not have any influence on the forthcoming instability analysis. This aspect will become evident later on.

3. Linear instability analysis

The linear instability analysis involves the superposition of perturbations in the form of normal modes to the basic state. As mentioned above, we impose normal modes independent of y. As a consequence, a convenient definition of the perturbed fields involves a streamfunction Ψ, namely

$$u(x,y,z,t) = u_b(z) + \varepsilon\,\frac{\partial \Psi(x,z,t)}{\partial z}, \quad v(x,y,z,t) = v_b(z) + \varepsilon\,V(x,z,t),$$
$$w(x,y,z,t) = -\varepsilon\,\frac{\partial \Psi(x,z,t)}{\partial x}, \quad T(x,y,z,t) = T_b(x,y,z) + \varepsilon\,\Theta(x,z,t), \tag{7}$$

so that the local mass balance is identically satisfied. In Eq. (7), ε is a perturbation parameter such that $|\varepsilon| \ll 1$. On using the y component of the local momentum balance (3), one can easily check that $V(x,z,t)$ is identically zero. The pressure perturbation can be ignored by rearranging the x and z components of the momentum balance. Thus,

by neglecting terms $O(\varepsilon^2)$, the linearised governing equations for the perturbations are obtained from (3), (5) and (7) and given by

$$\frac{\partial^2 \Psi}{\partial x^2} + a\,\frac{\partial^2 \Psi}{\partial z^2} + a\,\frac{\partial \Theta}{\partial x} = 0,$$
$$\frac{\partial \Theta}{\partial t} + \frac{\partial T_b}{\partial x}\,\frac{\partial \Psi}{\partial z} - \frac{\partial T_b}{\partial z}\,\frac{\partial \Psi}{\partial x} + u_b\,\frac{\partial \Theta}{\partial x} = \frac{\partial^2 \Theta}{\partial x^2} + \frac{\partial^2 \Theta}{\partial z^2},$$
$$z = 0, 1: \qquad \Psi = 0, \quad \frac{\partial \Theta}{\partial z} = 0. \tag{8}$$

As anticipated, no role is played by p_b in the linear analysis of instability based on Eq. (8).

3.1. Normal modes

Let us now employ Fourier modes to express the perturbations as

$$\Psi(x,z,t) = i\,f(z)\,e^{i\,(kx-\omega t)}\,e^{\eta\,t}, \qquad \Theta(x,z,t) = h(z)\,e^{i\,(kx-\omega t)}\,e^{\eta\,t}, \tag{9}$$

where k is the wavenumber, η is the temporal growth rate and ω is the angular frequency. On substituting (9) into (8), we obtain

$$a\,f'' - k^2\,f + a\,k\,h = 0,$$
$$h'' - \left(k^2 + i\,k\,F(z)\cos\varphi + \eta - i\,\omega\right) h - i\,\frac{2Ra\cos\varphi}{Pe}\,f' - k\,G(z)\,f = 0,$$
$$z = 0, 1: \qquad f = 0, \quad h' = 0. \tag{10}$$

By relying on the analysis carried out by Barletta [4] for the special case of an isotropic medium, we might conjecture that the anisotropy does not alter the result that longitudinal modes ($\varphi = \pi/2$) are the most effective in triggering the onset of instability. Thus, we could set $\varphi = \pi/2$ so that $u_b = 0$ and $\partial T_b/\partial x = 0$ as one can infer from (5). Through this simplification, the linear instability eigenvalue problem (10) becomes

$$a\,f'' - k^2\,f + a\,k\,h = 0,$$
$$h'' - \left(k^2 + \eta - i\,\omega\right) h - k\,G(z)\,f = 0,$$
$$z = 0, 1: \qquad f = 0, \quad h' = 0. \tag{11}$$

An important property of the eigenvalue problems (10) and (11) is their invariance under the transformation

$$Ra \to -Ra, \quad z \to 1 - z. \tag{12}$$

This result implies that we can limit our instability analysis to the case of wall heating, $Ra > 0$, whereas wall cooling, $Ra < 0$, does merely entail a z midplane reflection for the eigenfunctions (f, h).

For the sake of completeness, we will test the effect of the inclination angle φ on the onset of the linear instability to validate our conjecture that the longitudinal modes effectively lead to instability at the smallest values of Ra. Such a test will be carried out for some sample values of a and Pe in the forthcoming Section 3.2.

3.2. Numerical solution

The differential eigenvalue problem (11) can be solved numerically by utilising the shooting method [27,28]. The aim is the detection of the lowest neutral stability threshold in the (k, Ra) parametric plane, for prescribed input values of the wavenumber k, of the Péclet number Pe, of the inclination angle φ and of the anisotropy ratio a. The shooting method solution of a differential eigenvalue problem is implemented in the *Mathematica 14.0* software environment [29] via the function `ParametricNDSolveValue`. The determination of the neutral stability curve requires setting $\eta = 0$ in (11) and by introducing an extra scale-fixing condition which removes the scale invariance of the solution (f, h) of (11). Such an extra condition is chosen as $h(0) = 1$. The end point condition $h'(1) = 0$ can finally be used to determine both Ra and ω via a root finding tool provided by the function `FindRoot`.

First step to be taken is the analysis of the role played by the inclination angle φ in the determination of the neutral stability condition. The neutral stability curves, displayed in the (k, Ra) plane,

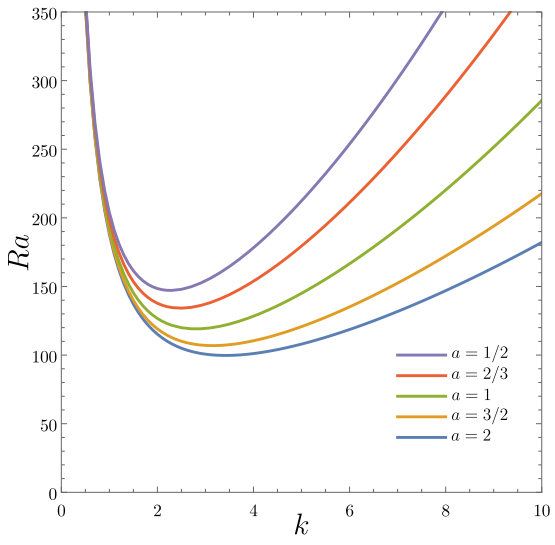

Fig. 3. Neutral stability curves for different anisotropy ratios a in the asymptotic case $Pe \gg 1$.

have a point of minimum Ra attained for a critical value of $k = k_c$. Such a minimum defines the critical values (k_c, Ra_c, ω_c) where, in particular, $Ra = Ra_c$ yields the lowest condition for the onset of the linear instability. Detecting, for prescribed Pe and a, the type of modes that trigger the onset of the instability means evaluating which inclination angle φ yields the smallest Ra_c. In every case examined, this analysis leads invariably to the result that the most unstable modes are longitudinal, *i.e.* corresponding to $\varphi = \pi/2$. Fig. 2 illustrates such a result by exploring the sample cases $Pe = 1000, 100, 50$ and 25 with different anisotropy ratios a. The most important feature displayed in Fig. 2 is the monotonically decreasing trend of the ratio between Ra_c and $Ra_{c,L}$ versus φ, where $Ra_{c,L}$ is the critical Rayleigh number relative to the longitudinal modes ($\varphi = \pi/2$). Thus, the longitudinal modes are the most unstable, as anticipated. In fact, the dependence on φ is extremely weak for $Pe = 1000$, whereas it gradually becomes more and more pronounced as Pe decreases. One may note that, in the case $Pe = 25$, the dependence on φ is remarkable and that no data are reported below $a = 1/4$. The reason is that there exists a minimal Pe, for every a, below which no linear instability is detected. Such a minimal Pe is larger than 25 for both $a = 1/5$ and $a = 1/10$. More details on this feature are reported in the forthcoming Section 4. A significant aspect in the evaluation of the role played by the inclination angle φ is that oblique modes $0 \le \varphi < \pi/2$ are endowed with a nonzero angular frequency at onset of the linear instability, while longitudinal modes are characterised by $\omega = 0$. Finally, we mention that the isotropic special case $a = 1$ has been included in Fig. 2 (dashed–dotted lines). As expected, the analysis of oblique modes for the isotropic case coincides with that provided in Barletta [4].

Having found a numerical support for the conjecture that longitudinal modes are the most unstable in every case, hereafter, the linear instability analysis will be entirely focussed on the longitudinal modes and, hence, on the solution of the stability eigenvalue problem (11).

4. Discussion of the results

Within the analysis of the longitudinal modes, there is an interesting asymptotic case which addresses flows with a large Péclet number, *i.e.*, $Pe \gg 1$. This case is easily identified in Eqs. (11) by letting $Ra^2/Pe^2 \to 0$ which means keeping a finite Ra with $Pe \to \infty$.

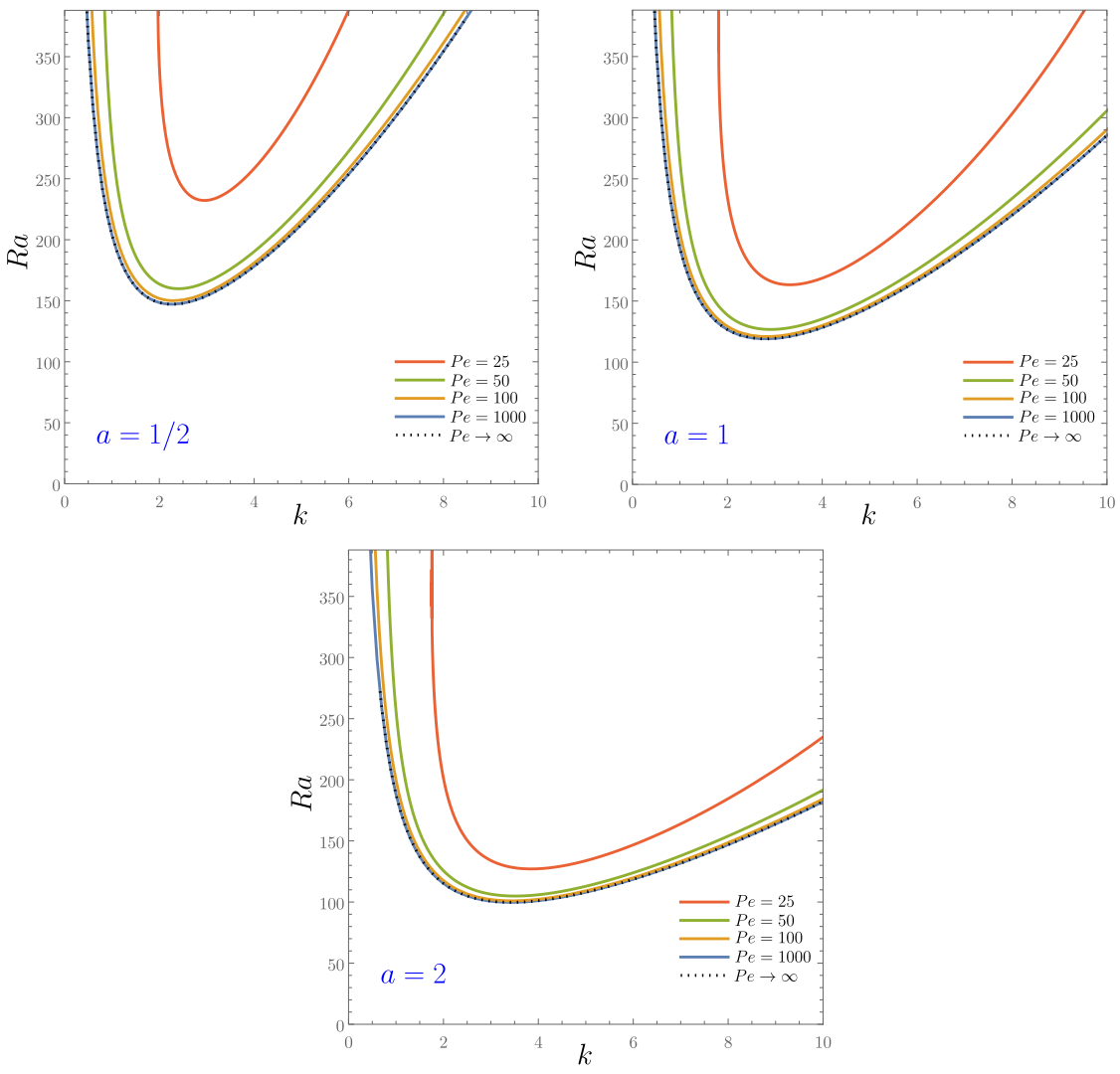

Fig. 4. Neutral stability curves for $a = 1/2, 1, 2$ and different Péclet numbers.

4.1. Neutral stability curves

The neutral stability curves for the asymptotic solution with $Pe \gg 1$ are displayed in Fig. 3 for different anisotropy ratios a. Relative to the isotropic case ($a = 1$), we easily detect a destabilisation when $a > 1$ and a stabilisation when $a < 1$. In fact, the unstable region in the (k, Ra) parametric plane is, in each case, above the neutral stability curve, with the minimum of the curve identifying the critical values (k_c, Ra_c). Thus, linear instability is possible only when $Ra > Ra_c$ and, from Fig. 3, one can easily conclude that Ra_c decreases with a, meaning an increasing instability. Such a phenomenon can be explained physically if one thinks that the larger is a the larger is the vertical permeability relative to the horizontal permeability. Undoubtedly, an improved permeability in the vertical direction tends to favour the development of buoyancy-induced convection cells and, hence, the onset of the instability.

Fig. 4 shows the destabilising effect of an increasing Péclet number with reference to the three sample cases $a = 1/2, 1$ and 2. It is also evident how the asymptotic case $Pe \gg 1$, *viz.* the mathematical limit $Pe \to \infty$, provides a fairly good approximation of the case $Pe = 1000$ or even of $Pe = 100$.

Up to this point, we have focussed our attention on the neutral stability curves as drawn in the (k, Ra) plane. Another important feature of the neutral stability condition, already mentioned in Section 3.2, is that $\omega = 0$, meaning that the transition to linear instability is driven by non-oscillatory longitudinal modes or, equivalently, that the principle of exchange of stabilities holds true.

Table 1
Critical values of k and Ra.

Pe	$a = 1/2$		$a = 1$		$a = 2$	
	k_c	Ra_c	k_c	Ra_c	k_c	Ra_c
25	2.95157	232.193	3.31888	163.326	3.85083	127.081
50	2.40635	159.844	2.90868	126.769	3.51080	104.888
100	2.30341	150.041	2.82692	120.866	3.44169	100.958
1000	2.27058	147.139	2.80097	119.081	3.41980	99.7531
∞	2.27025	147.110	2.80071	119.064	3.41958	99.7411

4.2. Critical values

Numerical data for the critical values k_c and Ra_c are provided in Table 1. This table shows the general influence of a and Pe on the onset of the linear instability, namely, that Ra_c is a decreasing function of both a and Pe. Fig. 5 also shows the trend of Ra_c versus a for different values of Pe including the asymptotic case $Pe \to \infty$. We mention that the case $Pe = 1000$ is not reported as it would look indistinguishable from the limit $Pe \to \infty$. We already mentioned the existence of a minimal value of Pe below which no linear instability is detected. Such a minimal value depends on a and it coincides with $Pe = 25$

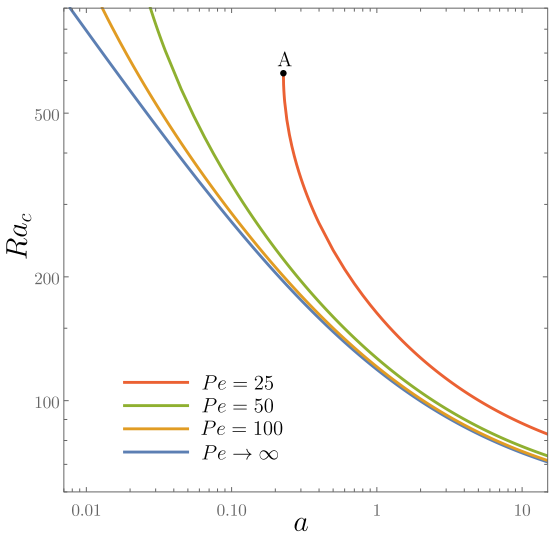

Fig. 5. Critical value of Ra versus a for different Péclet numbers. Point A is at $a = 0.227257$ and $Ra_c = 625.244$ and denotes the condition of minimum a below which no linear instability is detected at $Pe = 25$.

when $a = 0.227257$. This situation is denoted by point A in Fig. 5. In fact, the line with $Pe = 25$ is abruptly interrupted at point A having $Ra_c = 625.244$, as no linear instability is found with $a < 0.227257$.

4.3. Minimal Péclet number

A description of the minimal Peclét number feature of the linear instability transition is given by Fig. 6. In this figure, the minimum value of Pe needed for linear instability is plotted versus a so that the yellow region is that allowing the transition to linear instability, while the white region is that where no linear instability is detected. The right hand frame yields the critical Rayleigh number versus the minimal value of Pe. There is an interesting and simple approximate law that holds for the relation between such values of Ra_c and the minimal Pe, namely

$$Ra_c \approx Pe^2. \tag{13}$$

Such a feature have been pointed out by Barletta [4] for the isotropic case $a = 1$, but Fig. 6 shows that (13) holds for every a. Indeed, the right hand frame of Fig. 6 shows that the dashed black curve $Ra_c = Pe^2$ is almost perfectly superposed to the blue curve relative to the numerical values of Ra_c versus Pe. The point A in Fig. 6 is relative to the data for the isotropic case $a = 1$ which, in fact, are in perfect agreement with those reported in Barletta [4],

$$Pe = 19.1971, \quad k_c = 4.86457, \quad Ra_c = 368.456. \tag{14}$$

For the isotropic case, the shape of the neutral stability curves with Pe slightly larger than the minimal Péclet number value, $Pe = 19.1971$, had been already pointed out [4]. Indeed, the neutral stability curves become closed loops meaning islands of instability surrounded by a sea of linear stability in the parametric (k, Ra) plane. Eventually, when Pe reaches its minimal value for linear instability such loop-shaped curves shrink to a point and then disappear [4]. The same behaviour is illustrated in Figs. 7 and 8 for the anisotropic cases $a = 2$ and $a = 1/2$, respectively. These figures also show the point A where the closed loops of neutral stability ultimately collapse when Pe gradually decreases to its minimal value which is $Pe = 17.5264$ for $a = 2$ and $Pe = 21.4582$ for $a = 1/2$. The right hand frames of Figs. 7 and 8 show the trends of the growth rate η versus Ra along the constant k straight lines depicted in the left hand frames. Such plots are quite useful to suggest the meaning of the closed loops as islands of instability surrounded by a region of linear stability in the (k, Ra) parametric plane. In fact, these plots clearly show that crossing the loop region in the (k, Ra) plane with a fixed k and an increasing Ra yields a sign change of η from negative, meaning stability, to positive, meaning instability, and then negative again.

Table 2
Data for the condition of minimal Péclet number.

a	Pe	k	Ra
1/10	30.2013	2.74631	912.585
1/5	25.6948	3.25600	660.526
1/2	21.4582	4.08782	460.435
1	19.1971	4.86457	368.456
2	17.5264	5.79811	307.124
5	15.9770	7.33676	255.251
10	15.1627	8.80572	229.907

Table 2 finally collects some numerical data for the minimal Péclet number and the corresponding values of k and Ra for neutral stability at different anisotropy ratios a as compared to the isotropic case $a = 1$, whose numerical data have been already reported in (14).

5. Conclusions

The linear instability analysis of the mixed convection stationary flow in a uniformly heated or cooled porous channel has been carried out. The modelling of the momentum transfer has been based on Darcy's law and on the Oberbeck–Boussinesq approximation, by assuming anisotropy of the porous medium with a permeability in the vertical direction different from that in the horizontal directions. Thus, an anisotropy ratio a has been defined between the vertical and the horizontal permeabilities of the medium. Finally, the Rayleigh number Ra is proportional to the heat flux prescribed at the channel walls.

A basic stationary buoyant flow with parallel velocity field has been considered, with a flow rate parametrised by the Péclet number Pe.

The determination of the neutral stability condition for the onset of the linear instability has been accomplished by introducing normal mode perturbations. The resulting stability eigenvalue problem has been solved numerically by employing the shooting method. The main results obtained are the following:

- In every case considered, the most unstable modes turned out to be longitudinal, meaning that their wave vector is inclined an angle $\pi/2$ with respect to the basic flow direction.
- The analysis has been focussed on the longitudinal modes revealing that both parameters a and Pe have a destabilising effect. In other words, a vertical permeability larger than the horizontal permeability results in an instability at smaller Rayleigh numbers as expected by reasoning on purely physical grounds.
- The asymptotic numerical solution for $Pe \gg 1$ turned out to be a quite useful and reliable approximation for cases where $Pe > 100$. Such an approximation becomes gradually less accurate when a becomes significantly smaller than 1.
- There exists a minimal nonzero value of Pe for linear instability, for every prescribed anisotropy ratio a. No linear instability has been detected below such a Péclet number.
- Close to the minimal Péclet number, the neutral stability curves display a closed-loop shape and, eventually, they shrink to a point when the minimal Pe is approached from above.

Mixed convection flow in channels with uniform wall heating/cooling is of great importance for the description of heat transfer and its enhancement in heat exchangers. Nowadays, the use of metal foams in compact heat exchangers is a challenging frontier of industrial design. The system analysed in this paper is a simplified model of such type of situations, where an highly conducting porous medium saturated by a fluid provides the exchange area increase required for the intensification of heat transfer. The analysis conducted here is just the first

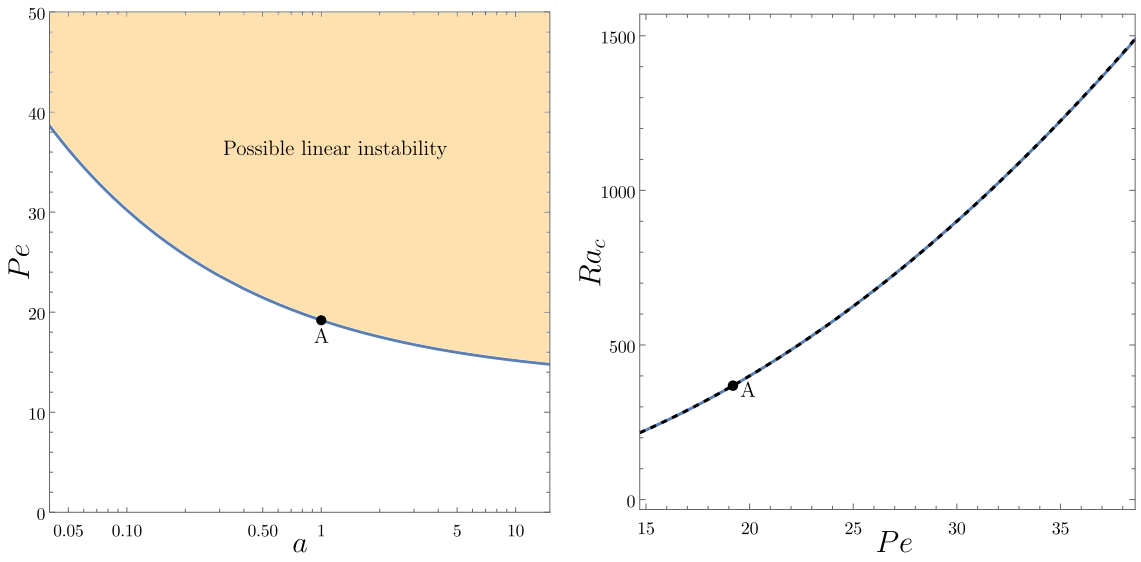

Fig. 6. Minimal value of Pe versus a for possible linear instability (left hand frame); critical value of Ra versus Pe at minimal Péclet number for instability (right hand frame). The black dashed line represents the $Ra_c = Pe^2$ law. Point A denotes the data for the isotropic case $a = 1$, Eq. (14).

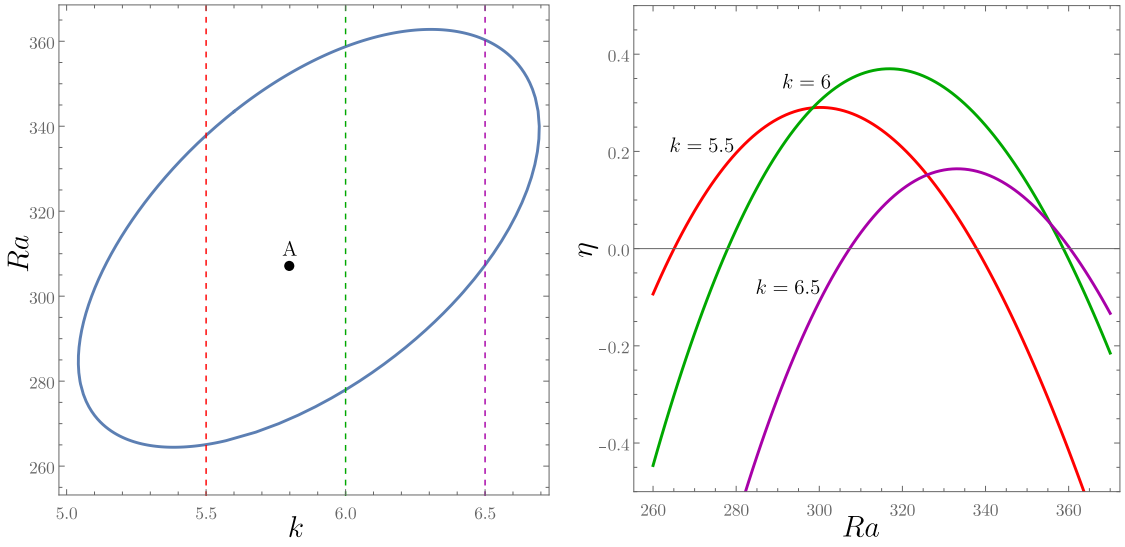

Fig. 7. Closed-loop neutral stability curve for $a = 2$ and $Pe = 17.6$ in the (k, Ra) plane (left hand side). Plots of the growth rate η versus Ra for $a = 2$, $Pe = 17.6$ and different wavenumbers k (right hand frame). The neutral stability locus at the minimal value of $Pe = 17.5264$ for $a = 2$, where the neutral stability curve shrinks to a point, is denoted with A.

step of further investigations that are specifically meant to explore the fully nonlinear behaviour of the cellular patterns predicted after the transition to instability. In particular, an opportunity for future research is the numerical evaluation of the Nusselt number and, hence, of the heat transfer coefficient resulting from the cellular flow superposed to the basic parallel velocity profile under supercritical conditions.

CRediT authorship contribution statement

A. Barletta: Writing – review & editing, Writing – original draft, Validation, Methodology, Investigation, Formal analysis, Conceptualization. **M. Celli:** Writing – review & editing, Writing – original draft, Validation, Methodology, Investigation, Formal analysis, Conceptualization. **P.V. Brandão:** Writing – review & editing, Writing – original draft, Validation, Methodology, Investigation, Formal analysis, Conceptualization. **S. Lazzari:** Writing – review & editing, Writing – original draft, Validation, Methodology, Investigation, Formal analysis, Conceptualization. **E. Ghedini:** Writing – review & editing, Writing – original draft, Validation, Methodology, Investigation, Formal analysis, Conceptualization.

Declaration of competing interest

The authors declare that they have no known competing financial interests or personal relationships that could have appeared to influence the work reported in this paper.

Data availability

No data was used for the research described in the article.

Acknowledgements

The work was supported by Alma Mater Studiorum Università di Bologna, Italy, grant number RFO-2023.

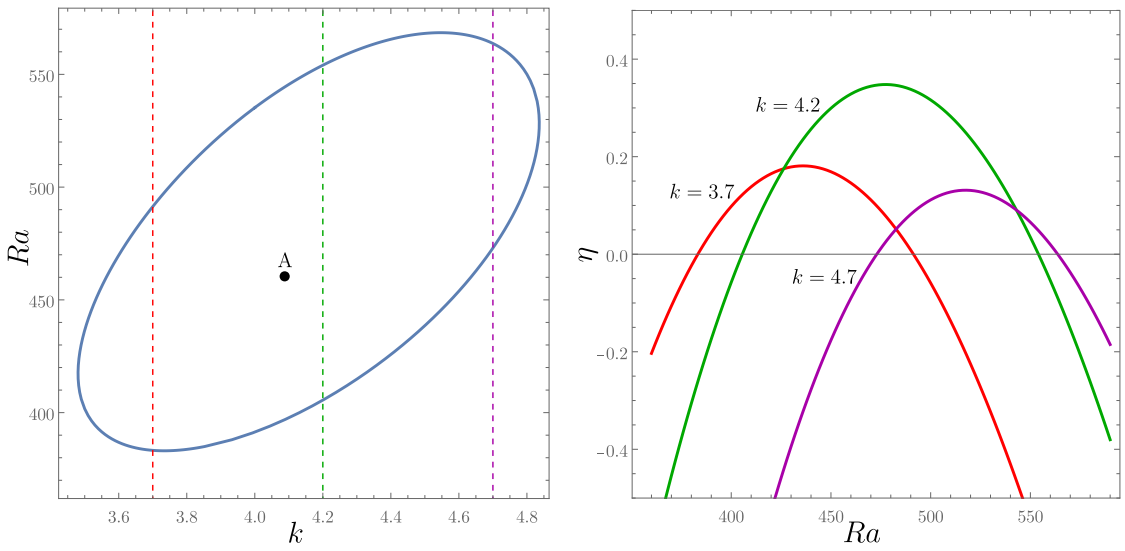

Fig. 8. Closed-loop neutral stability curve for $a = 1/2$ and $Pe = 21.6$ in the (k, Ra) plane (left hand side). Plots of the growth rate η versus Ra for $a = 1/2$, $Pe = 21.6$ and different wavenumbers k (right hand frame). The neutral stability locus at the minimal value of $Pe = 21.4582$ for $a = 1/2$, where the neutral stability curve shrinks to a point, is denoted with A.

References

[1] C.W. Horton, F.T. Rogers Jr., Convection currents in a porous medium, J. Appl. Phys. 16 (1945) 367–370.

[2] E.R. Lapwood, Convection of a fluid in a porous medium, Math. Proc. Cambridge Philos. Soc. 44 (1948) 508–521.

[3] M. Prats, The effect of horizontal fluid flow on thermally induced convection currents in porous mediums, J. Geophys. Res. 71 (1966) 4835–4838.

[4] A. Barletta, Thermal instability in a horizontal porous channel with horizontal through flow and symmetric wall heat fluxes, Transp. Porous Media 92 (2012) 419–437.

[5] L.A. Sphaier, A. Barletta, Unstable mixed convection in a heated horizontal porous channel, Int. J. Therm. Sci. 78 (2014) 77–89.

[6] A. Barletta, M. Celli, A.V. Kuznetsov, Convective instability of the Darcy flow in a horizontal layer with symmetric wall heat fluxes and local thermal nonequilibrium, ASME J. Heat Transf. 136 (2014) 012601.

[7] L.A. Sphaier, A. Barletta, M. Celli, Unstable mixed convection in a heated inclined porous channel, J. Fluid Mech. 778 (2015) 428–450.

[8] A. Barletta, D.A.S. Rees, Unstable mixed convection flow in a horizontal porous channel with uniform wall heat flux, Transp. Porous Media 129 (2019) 385–402.

[9] D.A. Nield, A. Bejan, Convection in Porous Media, fifth ed., Springer, New York, 2017.

[10] J.E. Weber, Convection in a porous medium with horizontal and vertical temperature gradients, Int. J. Heat Mass Transfer 17 (1974) 241–248.

[11] D.A. Nield, Convection in a porous medium with inclined temperature gradient, Int. J. Heat Mass Transfer 34 (1991) 87–92.

[12] D.A. Nield, Convection in a porous medium with inclined temperature gradient: additional results, Int. J. Heat Mass Transfer 37 (1994) 3021–3025.

[13] P.N. Kaloni, Z. Qiao, Non-linear stability of convection in a porous medium with inclined temperature gradient, Int. J. Heat Mass Transfer 40 (1997) 1611–1615.

[14] Z. Qiao, P.N. Kaloni, Convection in a porous medium induced by an inclined temperature gradient with mass flow, ASME J. Heat Transf. 119 (1997) 366–370.

[15] L. Storesletten, D.A.S. Rees, Onset of convection in an inclined anisotropic porous layer with internal heat generation, Fluids 4 (2) (2019) 75.

[16] B. Straughan, Anisotropic bidispersive convection, Proc. R. Soc. A 475 (2019) 20190206.

[17] C. Hemanthkumar, I.S. Shivakumara, B.M. Shankar, G. Pallavi, Exploration of anisotropy on nonlinear stability of thermohaline viscoelastic porous convection, Int. Commun. Heat Mass Transfer 126 (2021) 105427.

[18] F. Capone, M. Gentile, J.A. Gianfrani, Optimal stability thresholds in rotating fully anisotropic porous medium with LTNE, Transp. Porous Media 139 (2021) 185–201.

[19] F. Capone, J.A. Gianfrani, Natural convection in a fluid saturating an anisotropic porous medium in LTNE: effect of depth-dependent viscosity, Acta Mech. 233 (2022) 4535–4548.

[20] F. Capone, J.A. Gianfrani, Thermal convection for a Darcy-Brinkman rotating anisotropic porous layer in local thermal non-equilibrium, Ric. Mat. 71 (2022) 227–243.

[21] B. Straughan, Effect of anisotropy and boundary conditions on Darcy and Brinkman porous penetrative convection, Environ. Fluid Mech. 22 (2022) 1233–1252.

[22] R.K. Shah, A.L. London, Laminar flow forced convection in ducts, in: Advances in Heat Transfer, Academic Press, 1978.

[23] A. Barletta, The Boussinesq approximation for buoyant flows, Mech. Res. Commun. 124 (2022) 103939.

[24] P.A. Tyvand, L. Storesletten, Onset of convection in an anisotropic porous medium with oblique principal axes, J. Fluid Mech. 226 (1991) 371–382.

[25] M. Trew, R. McKibbin, Convection in anisotropic inclined porous layers, Transp. Porous Media 17 (1994) 271–283.

[26] A. Barletta, M. Celli, Anisotropy and the onset of the thermoconvective instability in a vertical porous layer, ASME J. Heat Transf. 143 (2021) 102601.

[27] B. Straughan, The Energy Method, Stability, and Nonlinear Convection, Springer, 2013.

[28] A. Barletta, Routes To Absolute Instability in Porous Media, Springer, 2019.

[29] Wolfram Research, Inc., Mathematica 14.0, 2024, https://www.wolfram.com/mathematica.